International Journal of Minerals, Metallurgy and Materials
Volume 24, Number 2, February 2017, Page 222
DOI: 10.1007/s12613-017-1399-0

High-temperature frictional wear behavior of MCrAlY-based coatings deposited by atmosphere plasma spraying

Chong Tao[1,2], *Lei Wang*[1], *and Xiu Song*[1]

1) Key Laboratory for Anisotropy and Texture of Materials (Ministry of Education), Northeastern University, Shenyang 110819, China
2) Baosteel Group Shanghai Meishan Iron & Steel Co. Ltd., Nanjing 210039, China
(Received: 11 June 2016; revised: 18 September 2016; accepted: 24 October 2016)

Abstract: Al_2O_3–Cr_2O_3/NiCoCrAlYTa coatings were prepared via atmosphere plasma spraying (APS). The microstructure and phase composition of the coatings were analyzed by X-ray diffraction (XRD), scanning electron microscopy (SEM), laser confocal scanning microscopy (LSCM), and transmission electron microscopy (TEM). The dry frictional wear behavior of the coatings at 500°C in static air was investigated and compared with that of 0Cr25Ni20 steel. The results show that the coatings comprise the slatted layers of oxide phases, unmelted particles, and pores. The hot abrasive resistance of the coatings is enhanced compared to that of 0Cr25Ni20, and their mass loss is approximately one-fifteenth that of 0Cr25Ni20 steel. The main wear failure mechanisms of the coatings are abrasive wear, fatigue wear, and adhesive wear.

Keywords: metal matrix composites; composite coatings; wear behavior; high temperature properties; plasma spraying

1. Introduction

Surface modification is an effective method to improve the friction and wear properties of metal components. At present, the main surface modification methods include thermal spraying, electroless plating, and ion implantation. Among these methods, atmosphere plasma spraying (APS) coatings have been well established as the protective barriers because APS provides an effective and economical way to deposit ceramic coatings. MCrAlY coatings have been used as the protective APS coatings against frictional wear at higher temperatures.

With the widespread use of metal matrix composite coatings in the field of high-temperature protective coatings, oxide ceramics dispersion-strengthened NiCoCrAlY coatings have been obtained through the introduction of hard oxide particles. This approach has become an important trend in improving the high-temperature wear resistance of MCrAlY coatings [1–6].

Many researchers have found that the ceramics are good potential reinforcement materials in MCoAlY coatings, and the coatings with good high-temperature frictional wear properties can be obtained by introducing other oxide particles. For example, NiCoCrAlY coatings containing Al_2O_3–B_4C exhibit good wear resistance from room temperature to 800°C and the main wear mechanism of coatings is abrasion wear [1]. As another example, researchers [7] have introduced CeO_2 into NiCrBSiFe coatings, resulting in the good wear performance at room temperature. Thus, the coatings with good high-temperature frictional wear properties can be obtained by introducing various oxide particles [8]. However, the strength of the coatings still needs improvement. Because the crystalline structures of Al_2O_3 and Cr_2O_3 are the same and the ionic radii of Al^{3+} and Cr^{3+} are similar to each other, Al_2O_3 and Cr_2O_3 easily form a solid solution. The coefficient of thermal expansion of NiCoCrAlYTa is similar to that of the base metal, which is beneficial for improving the bonding strength of the coatings. The high-temperature frictional wear behavior of micron Al_2O_3 partially stabilized by Cr_2O_3 dispersion-strengthened NiCoCrAlY coatings prepared using APS has not been previously reported. Therefore, in the present study, Cr_2O_3 and stabilized Al_2O_3 were used as reinforcements for NiCoCrAlY coatings. The microstructures, thermostability,

Corresponding author: Lei Wang E-mail: wanglei@mail.neu.edu.cn

and wear behavior of APS-sprayed Al_2O_3–Cr_2O_3/NiCoCrAlYTa were investigated, and the wear mechanism of the coatings was also discussed.

2. Experimental

2.1. Materials and APS thermal spraying process

Stainless steel 0Cr25Ni20 is an austenitic stainless steel with high chromium and nickel contents; it exhibits good oxidation and corrosion resistance. The Al_2O_3–Cr_2O_3/NiCoCrAlYTa coatings on the stainless steel 0Cr25Ni20 substrates were produced by APS, where three commercially available feedstock powders, i.e., Al_2O_3, Cr_2O_3, and NiCoCrAlYTa, were used. Fig. 1 shows the spherical morphology of these powders in sizes of 15–45 μm. Before the coating process, the stainless steel 0Cr25Ni20 substrates were degreased and grit blasted to a roughness of approximately 15 μm. The coatings were prepared using the aforementioned powders (70NiCoCrAlYTa–18Al_2O_3–12Cr_2O_3 (wt%)) in a commercial APS system (Prax-atmosphere-3710, USA). The coatings were deposited to a thickness of (180 ± 20) μm after six passes. The spraying parameters are shown in Table 1.

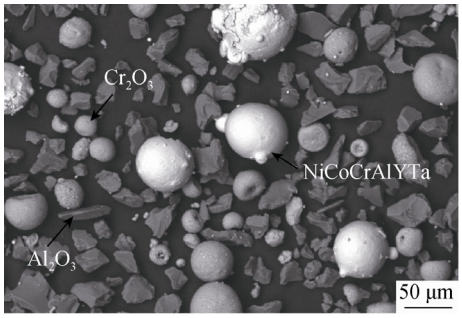

Fig. 1. Spherical morphology of the powders.

Table 1. Plasma spraying parameters

Arc gas flow rate / (L·min^{-1})	Secondary gas flow rate / (L·min^{-1})	Spray rate / (g·min^{-1})	Arc voltage / V	Arc current / A	Spraydistance / mm
55	18	45	40	500	80

The coatings were fabricated when the critical plasma spray parameter (CPSP) was 172; this parameter is strongly influenced by the volume fraction of the partially melted particulate structure as the following equation [9–11].

$$\mathrm{CPSP} = \frac{E \cdot I}{0.47v} \tag{1}$$

where E represents the voltage (V), I the current (A), and v the flow rate of primary gas (Ar) (L·min^{-1}).

The Vickers microhardness of the coatings and substrates was tested by indentation method. The microstructures of the coatings were characterized by X-ray diffraction (XRD; Bruker D8-Advanced, Germany), scanning electron microscopy (SEM; JEOL 6510A, Japan), and transmission electron microscopy (TEM; FEI TecnaiG2 20, USA).

2.2. Frictional wear tests at elevated temperatures

The friction and wear characteristics of the coatings were investigated using an MG-2000 configured in pin-on-disc arrangement under dry sliding at high temperature. A schematic of the tester is shown in Fig. 2. The pin size was ϕ6 mm × 12 mm. GCr15 was used as the friction pair in size of ϕ70 mm × 12 mm, whose hardness was approximately 60 HRC. The tests were performed at 500°C in static air. The load force (P) was installed at 10 N, and the sliding speed (V) was adjusted to 250 r/s. The total sliding rounds were 1500, 3000, and 4500 r. At least three parallel samples were tested for each coating to obtain the average mass loss.

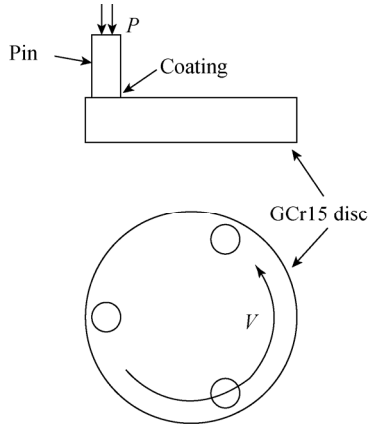

Fig. 2. Schematic illustration of the pin-on-disc friction and wear test.

Before the testing, the samples were cleaned with acetone. An FA2004 analytical balance with a precision of 10^{-1} mg was used to measure the sample mass before and after the frictional wear testing. The wear mass loss rate (W_L) was calculated as

$$W_L = \frac{\Delta w_i}{t} = \frac{w_i - w_0}{t} \tag{2}$$

where i is the number of wear rounds, w_i the sample mass after wear, and w_0 is the sample mass before wear. High-temperature frictional wear behavior curves were constructed after the wear tests, showing the mass loss as a function of the number of wear rounds. The morphology of

the wear scars was characterized by SEM, laser confocal scanning microscopy (LSCM; Olympus Lext 3100, Japan), and energy-dispersive X-ray spectroscopy (EDS; Oxford Incax Sights, England).

3. Results and discussion

3.1. Phase composition

Fig. 3 presents the XRD patterns of the feedstock powder and the as-sprayed coating before and after wear test. The XRD pattern of the feedstock powder indicates that Cr_2O_3, Ni_3Al, and Al_2O_3 are present. However, an amorphous/nanocrystalline Cr_2O_3 and Al_2O_3 phase ($2\theta \approx 45°$) forms during the APS process because of the high flame temperature and high cooling velocity. A similar phase has been mentioned in previous Refs. [12–14]. In addition, after the wear tests, an amorphous/nanocrystalline phase is detected in the coating, which indicates that the temperature of wearing is lower than the crystallization temperature of the coating.

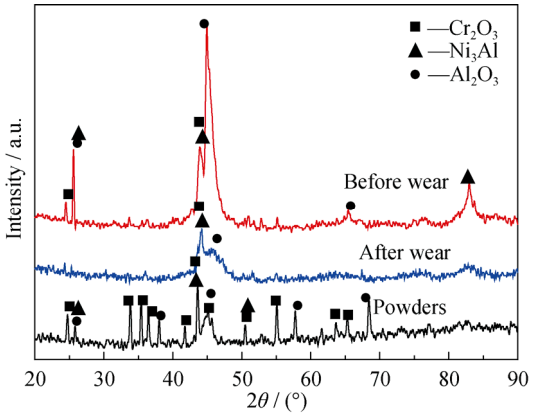

Fig. 3. XRD patterns of the feedstock powder and the as-sprayed coating before and after wear testing.

The partial amorphization was confirmed by TEM images and the corresponding selected-area electron diffraction (SAED) pattern is shown in Fig. 4. The MCrAlY-based alloy system usually includes multiple components with substantial atomic size mismatches and suitable negative heats of mixing among the constituent elements [15]. In addition, a cooling rate of splats that exceeds 10^6 K·s^{-1} during APS processes is beneficial to the formation of an amorphous phase [16].

3.2. Characterization of the coatings

Fig. 5 shows the transverse section of the as-sprayed coatings. The low magnification of Fig. 5(a) reveals that the coating is dense and well bonded to the substrate, with a thickness of 300 μm. The coating exhibits a lamellar structure almost paralleling the interface between the coating and substrate. In addition, some melted or semi-melted particles and microcracks are observed, as marked by black arrows in Fig. 5(b); these features are consequences of the high-velocity spray and high melting point of the powders. Characteristics typical of plasma-sprayed coatings, such as holes, cracks, and partially melted or semi-molten particles, are also observed. This structure is useful for improving the coating toughness [17–19]. The average porosity of the coating is approximately 15.06%. The average microhardness is $Hv_{0.1}$ 413, which is approximately two times that of the substrate ($HV_{0.1}$ 200), as shown in Fig. 6.

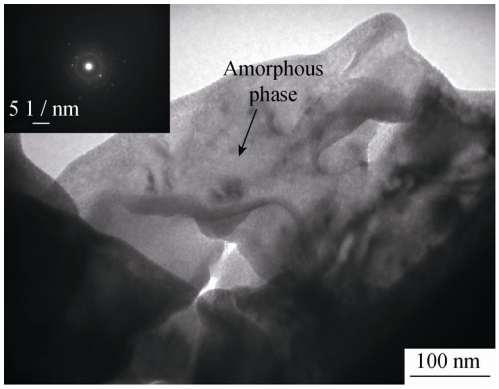

Fig. 4. TEM image and SAED pattern of the amorphous phase.

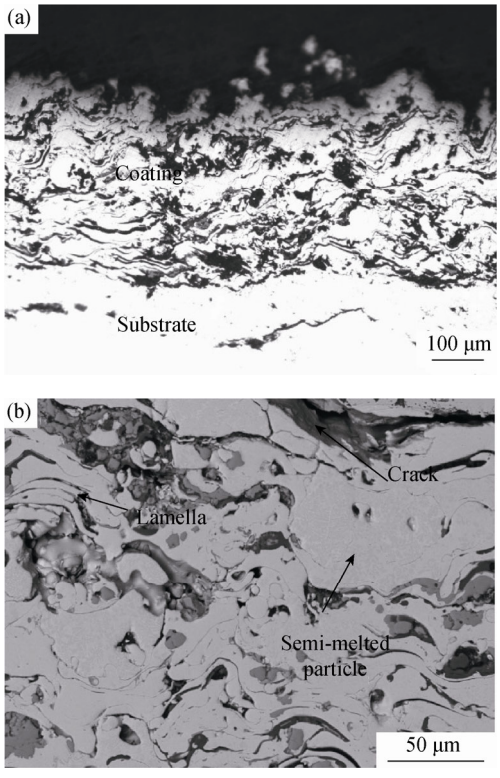

Fig. 5. Transverse section images of the as-sprayed coating.

3.3. Frictional wear behavior of coatings

Fig. 7 shows the mass loss of the coating and 0Cr25Ni20 stainless steel at different wear distances. The results show that the mass loss of the coating is relatively stable throughout the test. After 3000 r, the mass loss increases slightly. By contrast, the mass loss of 0Cr25Ni20 increases from the beginning, and then increases faster after 3000 r; the mass loss of the 0Cr25Ni20 substrate is almost fifteen times greater than that of the coating.

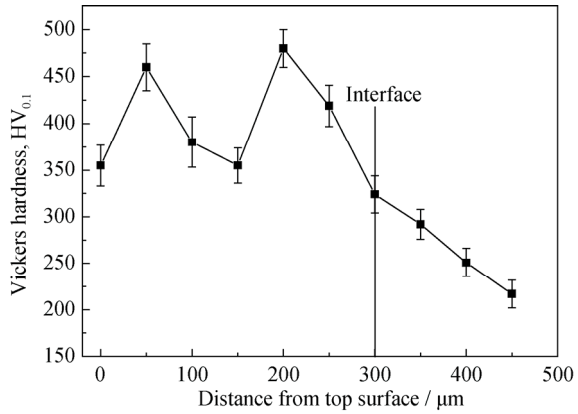

Fig. 6. Curve of hardness vs. distance from the top surface for the coating.

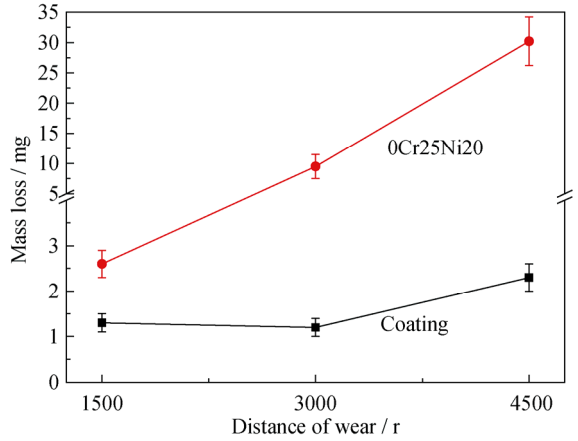

Fig. 7. Comparison of wear loss in mass.

The surface morphologies of the coatings after different rounds are shown in Fig. 8. After 1500 r, the coating surface does not substantially differ from the original coating surface. Some holes and peak-like protrusions are well preserved. As shown in Figs. 8(c) and (d), the original peak-like protrusions are almost non-existent on the coating surface, but the surface contains numerous furrows. In Figs. 8(e) and (f), the surface is smoother than before; no peaks or furrows are observed. In addition, the wear mechanism of the coatings is mainly abrasive wear, fatigue wear, and adhesive wear [20–21].

Fig. 9 shows the high-magnification SEM images of the coating surfaces after different numbers of wear-testing rounds. Fig. 9(a) reveals that, after 1500 r, the wear surface of the coating is smooth. Few cracks and non-particle pull-out are observed; however, the surface contains many superficial furrows parallel to the sliding direction. The coating shows good wear resistance in the initial friction stage at high temperature. This result suggests that the coating is slightly plastically deformed under this condition. Fig. 9(b) shows that the oxygen content is as high as 59.82at%, indicating that oxidizing reactions occur on the coating surface.

As shown in Fig. 9(c), after 3000 r, many pits with different sizes and thin superficial scratches are observed in the sliding direction; some cracks are also evident. EDS spectra in Fig. 9(d) results reveal that numerous aluminum oxide particles are present on the coating surface, which may improve the wear resistance of the coatings. Thus, after 3000 r, the wear mechanism becomes microfracture and fatigue wear.

After 4500 r of wear (Fig. 9(e)), the pits are filled with abrasive dusts and no large cracks are observed. As shown in Fig. 9(f), Fe has been transferred to the coating surface from the friction pair, and the mass fraction is approximately 41.30%. The wear mechanism after 4500 r of wear is adhesive wear.

The coating, which has a unique structure, can not only absorb crack growth energy but also prevent crack generation and migration, resulting in improved toughness and wear resistance. When the coating is sliding with GCr15 steel, the hardness of NiCoCrAlYTa, which is the binding phase, is very low, resulting in the coating furrowing and cutting wore first. As a result, the hard phase of oxide ceramics is exposed to the coating surface and contacts with the friction pair directly at a certain angle under periodic cycles. At this point, the force on the oxide ceramic particles can be decomposed into a vertical force and a parallel force. The vertical force presses the oxide particles into the coating, and the parallel force causes the oxide particles to undergo tangential movement. When the oxide particles are pressed by GCr15 steel and make a relative motion along the coating surface, abrasions and microcuttings are generated on the coating surface in the same direction as the friction. The exposed oxide particles under a periodic vertical force are easily crushed, resulting in the particles fracturing and loosening. When the parallel force exceeds the bonding strength of the coating, the particles are pulled from the coating surface, resulting in small pits.

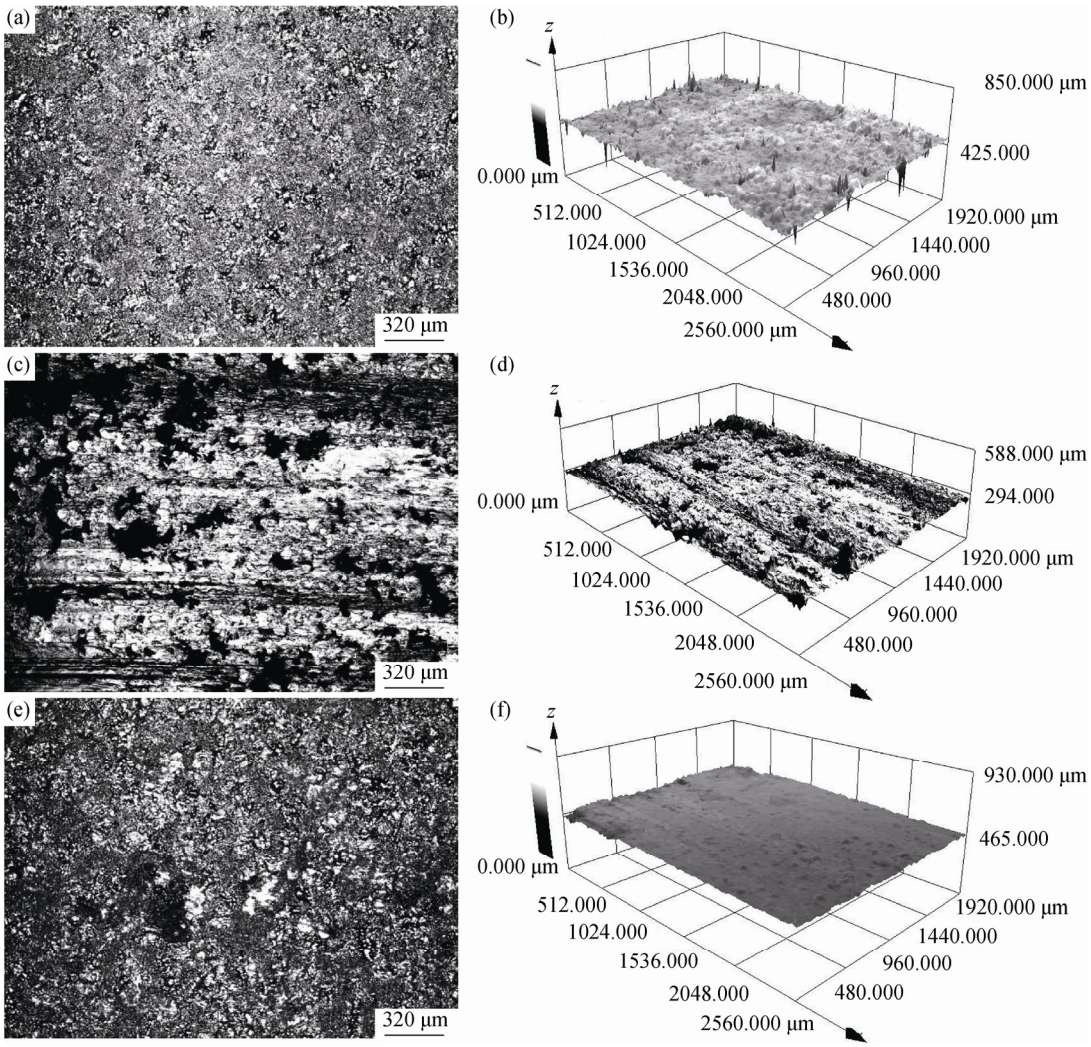

Fig. 8. SEM and LSCM micrographs of the coating worn surfaces: (a,b) after 1500 r; (c,d) after 3000 r; (e,f) after 4500 r.

Fig. 9(c) shows that, when the oxide particles are pulled out, the fine disperse particles are not fully integrated with the bonded phase. Moreover, the coating's microstructure is loose. Because the oxide particles and the metal bonding phase are not very similar, numerous flaws are created, which contribute to weaker bonding. The oxide particles near these flaws are easily pulled out during the friction process of wear testing. Fig. 9(e) shows the scratches formed by two different mechanisms. In the first case, a particle spalling pit is observed at the end of the scratch, indicating that the scratch is formed by the microcutting of the hard phase of the oxide particles when they are pulled from the coating surface. In the second case, the pits do not appear at the scratches, indicating that, after a long-term interaction between the GCr15 and coating, the scratches are formed by the hard microbulges on the GCr15 surface under fatigue wear. Another reason for scratch formation is that, in the process of relative sliding, the hard phase of pulled-out oxide particles or chippings scratches the coating surface under pressure, which is abrasive wear.

4. Conclusions

(1) The Al_2O_3–Cr_2O_3/NiCoCrAlYTa coatings have a uniform microstructure and tight semi-metallurgical bonding to the substrates. The coatings consist of an amorphous phase and several kinds of oxides such as Cr_2O_3, Ni_3Al, and Al_2O_3. The average porosity of the coatings is 15.06%. The average microhardness is $Hv_{0.1}$ 413, which is approximately two times that of the substrate ($Hv_{0.1}$ 200).

(2) The frictional wear resistance of the Al_2O_3–Cr_2O_3/NiCoCrAlYTa coatings is better than that of the 0Cr25Ni20 substrates at 500°C under non-lubrication friction. After 3000 r of friction wear, the mass loss of the Al_2O_3–Cr_2O_3/NiCoCrAlYTa coatings is only one-fifteenth that of 0Cr25Ni20.

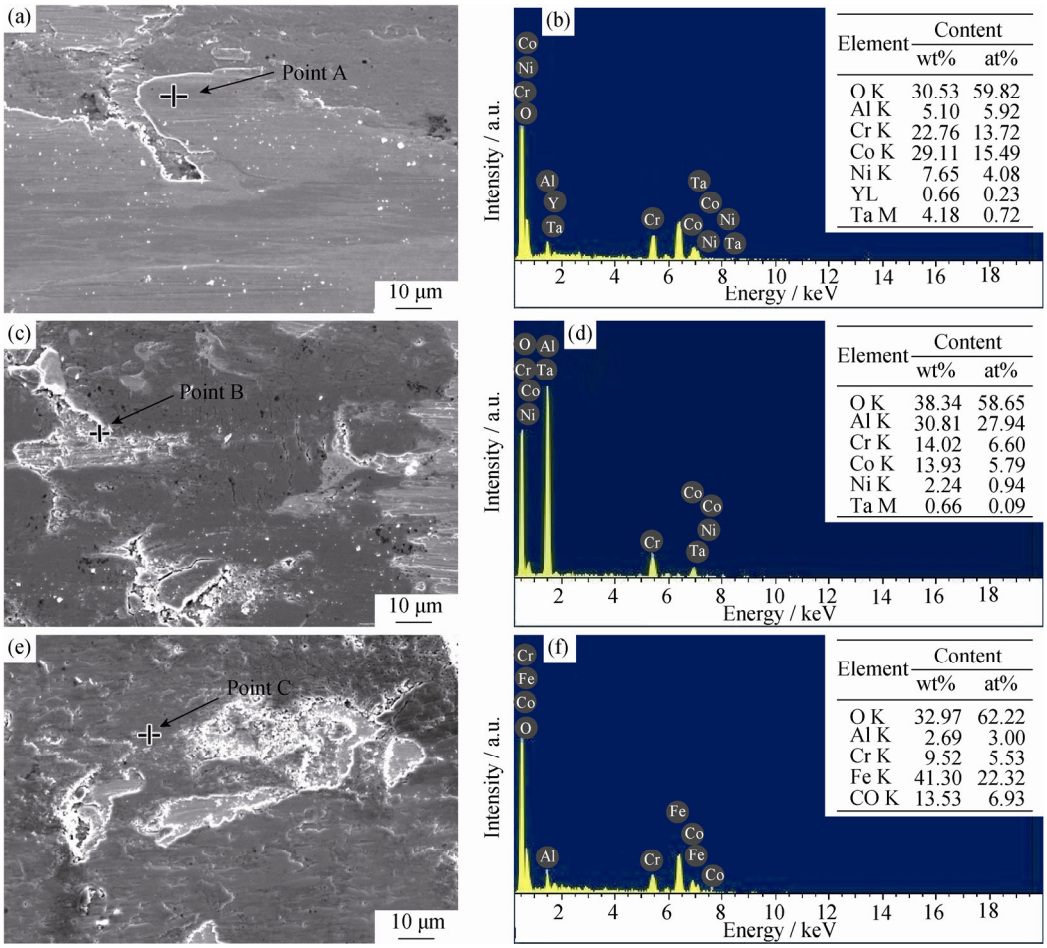

Fig. 9. SEM images and EDS spectra of the coating worn surface: (a,b) after 1500 r; (c,d) after 3000 r; (e,f) after 4500 r.

(3) Under the condition of high temperature and non-lubrication friction, the main wear failure mechanisms of the Al_2O_3–Cr_2O_3/NiCoCrAlYTa coatings are abrasive wear, fatigue wear, and adhesive wear.

Acknowledgements

This work was financially supported by the National High-tech Research and Development Program of China (No. 2012AA03A513), the Fundamental Research Funds for the Central Universities (No. N140204001), and the National Natural Science Foundation of China (Nos. 51371044 and 51301037).

References

[1] Y. Cao, C. Huang, W. Liu, W. Zhang, and L. Du, Effects of boron carbide content on the microstructure and properties of atmospheric plasma-sprayed NiCoCrAlY/Al_2O_3–B_4C composite coatings, *J. Therm. Spray Technol.*, 23(2014), No. 4, p. 716.

[2] K. Bobzin, T. Schläfer, K. Richardt, and M. Brühl, Development of oxide dispersion strengthened MCrAlY coatings, *J. Therm. Spray Technol.*, 17(2008), No. 5, p. 853.

[3] T. Zhang, C. Huang, H. Lan, L. Du, and W. Zhang, Oxidation and hot corrosion behavior of plasma-sprayed MCrAlY–Cr_2O_3 coatings, *J. Therm. Spray Technol.*, 25(2016), No. 6, p. 1208.

[4] E. Bahadori, S. Javadpour, M. Shariat, and F. Mahzoon, Preparation and properties of ceramic Al_2O_3 coating as TBCs on MCrAly layer applied on Inconel alloy by cathodic plasma electrolytic deposition, *Surf. Coat. Technol.*, 228(2013), p. S611.

[5] G. Pulci, J. Tirillò, F. Marra, F. Sarasini, A. Bellucci, T. Valente, and C. Bartuli, High temperature oxidation of MCrAlY coatings modified by Al_2O_3 PVD overlay, *Surf. Coat. Technol.*, 268(2015), p. 198.

[6] P. Ren, S. Zhu, and F. Wang, Spontaneous reaction formation of $Cr_{23}C_6$ diffusion barrier layer between nanocrystalline MCrAlY coating and Ni-base superalloy at high temperature, *Corros. Sci.*, 99(2015), p. 219.

[7] M. Li, S. Zhang, H. Li, Y. He, J.H. Yoon, and T.Y. Cho, Effect of nano-CeO_2 on cobalt-based alloy laser coatings, *J. Mater. Process. Technol.*, 202(2008), No. 1-3, p. 107.

[8] P. Ganapathy, G. Manivasagam, A. Rajamanickam, and A. Natarajan, Wear studies on plasma-sprayed Al_2O_3 and 8mole% of Yttrium-stabilized ZrO_2 composite coating on biomedical Ti–6Al–4V alloy for orthopedic joint application, *Int. J. Nanomed.*, 10(2015), Suppl. 1, p. 213.

[9] D. Zhao, F. Luo, W. Zhou, and D. Zhu, Effect of critical plasma spray parameter on complex permittivity and microstructure by plasma spraying Cr/Al_2O_3 coatings, *Appl. Surf. Sci.*, 264(2013), p. 545.

[10] S.T. Aruna, N. Balaji, J. Shedthi, and V.K.W. Grips, Effect of critical plasma spray parameters on the microstructure, microhardness and wear and corrosion resistance of plasma sprayed alumina coatings, *Surf. Coat. Technol.*, 208(2012), p. 92.

[11] S. Yugeswaran, V. Selvarajan, M. Vijay, P.V. Ananthapadmanabhan, and K.P. Sreekumar, Influence of critical plasma spraying parameter (CPSP) on plasma sprayed alumina–titania composite coatings, *Ceram. Int.*, 36(2010), No. 1, p. 141.

[12] Y. Gao, Y. Zhao, D. Yang, and J. Gao, A nvel plasma-sprayed nanostructured coating with agglomerated-unsintered feedstock, *J. Therm. Spray Technol.*, 25(2016), No. 1, p. 291.

[13] M.M. Machado-López, J. Faure, M.A. Espinosa-Medina, M.I. Espitia-Cabrera, and M.E. Contreras-García, Enhanced corrosion resistance in artificial saliva of Ti_6Al_4V with ZrO_2 nanostructured coating, *J. Electrochem. Soc.*, 162(2015), No. 11, p. D3090.

[14] H. Jamali, R. Mozafarinia, R.S. Razavi, and R. Ahmadi-Pidani, Comparison of thermal shock resistances of plasma-sprayed nanostructured and conventional yttria stabilized zirconia thermal barrier coatings, *Ceram. Int.*, 38(2012), No. 8, p. 6705.

[15] B.F. Lu, L.T. Kong, Z. Jiang, Y.Y. Huang, J.F. Li, and Y.H. Zhou, Roles of alloying additions on local structure and glass-forming ability of Cu–Zr metallic glasses, *J. Mater. Sci.*, 49(2014), No. 2, p. 496.

[16] J.Y. Cho, S.H. Zhang, T.Y. Cho, J.H. Yoon, Y.K. Joo, and S.K. Hur, The processing optimization and property evaluations of HVOF Co-base alloy T800 coating, *J. Mater. Sci.*, 44(2009), No. 23, p. 6348.

[17] D. Kumar, K.N. Pandey, and D.K. Das, Microstructure studies of air-plasma-spray-deposited CoNiCrAlY coatings before and after thermal cyclic loading for high-temperature application, *Int. J. Miner. Metall. Mater.*, 23(2016), No. 8, p. 934.

[18] C. Lamuta, G.D. Girolamo, and L. Pagnotta, Microstructural, mechanical and tribological properties of nanostructured YSZ coatings produced with different APS process parameters, *Ceram. Int.*, 41(2015), No. 7, p. 8904.

[19] C. Tao, L. Wang, N. Cheng, H. Hu, Y. Liu, and X. Song, Hot corrosion performance of AlO–CrO/NiCoCrAlYTa and AlO/NiCoCrAlYTa coatings deposited by atmospheric plasma spraying, *J. Therm. Spray Technol.*, 25(2016), No. 4, p. 797.

[20] Y. Zhou, Q.Y. Zhang, J.Q. Liu, X.H. Cui, J.G. Mo, and S.Q. Wang, Wear characteristics of a thermally oxidized and vacuum diffusion heat treated coating on Ti–6Al–4V alloy, *Wear*, 344-345(2015), p. 9.

[21] K. Aslantas, I. Ucun, and A. Çicek, Tool life and wear mechanism of coated and uncoated Al_2O_3/TiCN mixed ceramic tools in turning hardened alloy steel, *Wear*, 274-275(2012), p. 442.